Journal of the Korean Society of Marine Environment & Safety
Research Paper
Vol. 25, No. 3, pp. 366-372, May 31, 2019, ISSN 1229-3431(Print) / ISSN 2287-3341(Online) https://doi.org/10.7837/kosomes.2019.25.3.366

Motion Behavior of Platform Supply Vessels Running Under Regular Wave Conditions in RANS Model

Huiseung Park* · Hoyun Jang**† · Namhyun Ahn*** · Hyunsik Yoon****

*, ** Green-ship Research Division, Research Institute of Medium and Small Shipbuiling, 46757, Busan, Korea
*** Department of Naval Architecture & Ocean Engineering, Koje College, 593325, Geoje, Korea
**** Department of Naval Architecture & Ocean Engineering, Pusan National University, 46241, Busan, Korea

Abstract : *This study performed a numerical analysis of a 3D unsteady viscous flow in order to investigate ship motion responses running through regular waves of the platform supply vessel. The feasibility of numerical analysis was tested under the three regular wave conditions of the KRISO container ship (KCS) suggested at the 2010 Gothenburg CFD Workshop. The resulting resistance coefficient, heave motion, and pitch angle were compared with the model test of the harmonic analysis. Also, the ship motion response characteristics of the platform supply vessel were performed using the proven method of the KRISO container ship (KCS). The ship motions including the resistance coefficient, heave motion, and pitch angle according to the time series were investigated via harmonic analysis under regular waves condition of λ/LPP=1.87 and H_S=0.078m*

Key Words : *Ship motion, Computational Fluid Dynamics (CFD), Regular wave, Finite volume method (FVM), Heave motion, Pitch angle*

1. Introduction

An offshore support vessel (OSV) is necessary throughout the life cycle of an offshore plant and is particularly essential for the offshore plant service industry. Various OSV types are needed according to the plant life cycle, and different OSV feet are organized due to the size of mines or offshore plants. The vessels performing key offshore functions are the most basic types of OSV, and include the anchor handling tug supply (AHTS) and platform supply vessel (PSV). Such vessels are utilized throughout the offshore plant life cycle, except during the exploration stage and different OSVs are supplied at different stages.

There are various types of OSVs, a term used for those vessels supporting the drilling of oil and gas, installation of production platforms, operations and maintenance, transportation, dismantling, etc. offshore. It performs direct support for the offshore plant, or various undersea works in a rough marine environment. The shape and installed equipment of OSV's differs widely, according to the purpose of the vessels and type of work to be performed. Functions of OSV's can be generally categorized into support, deep sea work and construction support, heavy cargo transport, vessel crew amenities and residential, exploration functions, etc.

* First Author : hspark@rims.re.kr, 051-974-5584
† Corresponding Author : hyjang@rims.re.kr, 051-974-5581

Unlike the depressed commercial vessel market following the recent global economic crisis, the demand for offshore plants and supporting assets is rapidly increasing. As such, the market for OSVs like the PSV, which supplies the materials like fuel, food and beverages, chemicals, etc., are needed for offshore platforms as well as transporting wastes such as wastewater and mud generated during drilling to the land (Park et al., 2015).

The PSV loads cargo, such as pipes in the space on the deck while the mud, cement, clear water, and fuel oil needed for drilling is all placed in the space below the deck. The liquid freight is transported in special pressurized tanks and equipment. The liquid or powder freight is pneumatically pumped and transported by the rig or platform. These transported materials include the dry powder, cement, water for drilling, oil or liquid mud, methanol, and other chemicals for special purposes.

The classification of a PSV consists of the dead weight (DWT) and size of the deck. Generally, a vessel of 3,000 DWT and 750 m^2 or larger deck size is considered as intermediate grade, while a vessel of 4,000 DWT and 900 m^2 or larger deck size is considered as large grade. Moreover, since a tank loads different types of cargo, the cargo tank capacity conforming to transport purposes such as dry bulk, clear water, fuel oil, brine, and lubricant can also be the important factors (Korea Maritime Institute, 2012).

The key technologies of such PSVs include optimum design

technology, vessel performance enhancement technology and safe navigation evaluation technology, risk based optimum design condition deductions, cargo window design technology, ice load and ice collision modeling and analysis, optimum vessel form and propulsion systems, etc. However, the technological level in Korea is less than 50 % that of what is found advanced countries, and thus PSV technologies solely depend upon imported technologies.

Recently the standard hull form design of a PSV was suggested for optimization (Yum et al., 2018), but other studies on the PSV vessel are still very few in number. This study performed numeric analysis so as to investigate the performance of running in regular waves of the PSV's which navigate various sea conditions. To obtain the feasibility of numeric analysis, the result were compared with the results of model tests of forward moving KCS in regular waves, as suggested at the 2010 Gothenburg CFD Workshop (Larsson et al., 2010).

2. Numerical Analysis Method

2.1 Governing Equation & Analysis Methods

This study used Star-CCM+, a general purpose program based on the finite volume method, to numerically analyze the heave motion and pitch angle of a PSV in regular wave conditions. It was assumed that there was a 3D transient incompressible viscous flow. Equations (1) and (2) represent the corresponding dominant equations, which are the continuity equation and Reynolds averaged Navier-Stokes (RANS) equation, respectively.

$$\frac{\partial u_i}{\partial x_i} = 0 \tag{1}$$

$$\frac{\partial(\rho u_i)}{\partial t} + \frac{\partial(\rho u_i u_j)}{\partial x_j} = -\frac{\partial p}{\partial x_i} + \frac{\partial}{\partial x_j}(-\overline{\rho u_i' u_j'}) + \frac{\partial}{\partial x_i}[\mu(\frac{\partial u_i}{\partial x_i} + \frac{\partial u_j}{\partial x_i})] + \rho g_i + F_i \tag{2}$$

Here, x_i, u_i, p, g_i, ρ and μ represent the Cartesian coordinate system, velocity components, pressure, acceleration of gravity, density, and viscosity while Fi means the external force. $\overline{\rho u_i' u_j'}$ from Equation (2) represents the Reynolds stress and is calculated using the realizable κ-ε model. The SIMPLE method was used for the velocity and pressure coupling. The convection term and diffusion term used the second order upstream difference method, and the second order central difference method, respectively. Two-phase, which features difference phases around the vessel body, was assumed. The volume of fluid (VOF) method was used to track the interface of the fluid.

2.2 Ship Motion Equation

The 6 DOF movement of the vessel is represented by Equation (3), which calculates the linear momentum consisting of the surging, swaying, and heaving. Equation (4) calculates the angular momentum consisting of rolling, pitching and yawing.

$$F_{CGi} = m\frac{d^2 x_{CGi}}{\partial t^2} \tag{3}$$

$$L_{CGi} = \frac{d}{dt}(I_{ij}\frac{d\theta_{CGi}}{\partial t}) \tag{4}$$

Here, F_{CG} and L_{CG} represent the forces applied to the center of gravity (CG) of the vessel and momentum component in i direction, respectively. m and I_{ij} represent the mass and moment of inertia, respectively while x_{CG} and Θ_{CG} represent the displacement of the translational motion and rotational motion, respectively. This study assumed 2DOF in observation of the heave motion and pitch angle only of forward moving vessels.

2.3 Numerical Verification

This study verified the feasibility of numeric analysis technique before investigating the motion performance of a PSV. The vessel used for verification was a KCS with a scale ratio of 52.6 (Tahara and Ando, 2000). The model test results of this KCS hull were provided as verification for the results of the numeric analysis conducted by each agency participating in the 2010 Gothenburg CFD Workshop (Larsson et al., 2010). In this paper, the verification data was measured by Force Technology in Denmark (Otzen et al., 2008).

Fig. 1 and Table 1 show the principal particulars of KCS, used to verify the numeric analysis. Table 2 presents the velocity, wave length, and wave height of each test. The coordinate system of the numeric analysis assumed the forward direction to be the x-axis, transverse direction to be the y-axis, and height to be the z-axis.

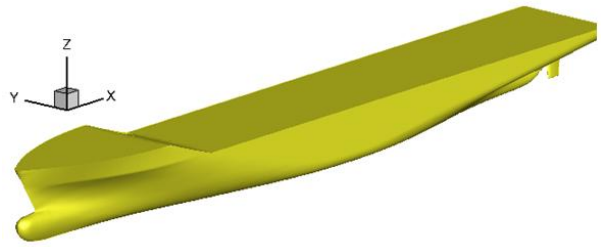

Fig. 1. KCS Model.

Table 1. Main particulars of KCS

KCS (Scale ratio = 52.667)		
Length	L_{PP}	4.3671 m
Draft	T	0.2051 m
Beam	B	0.6114 m
Watted surface area	S_W	3.3975 m^2
Block coefficient	C_B	0.615
LCB (%L_{PP}), fwd+	-	-1.48
Moment of inertia	k_{XX}/L_{PP}	0.40
Moment of inertia	k_{YY}/L_{PP}, k_{ZZ}/L_{PP}	0.25

Table 2. Test cases in regular waves for KCS

Condition		C2	C3	C4
Speed (m/s)	V	1.701	1.701	2.151
Froude number	Fn	0.26	0.26	0.33
Reynolds number	Rn	6.52×10^6	6.52×10^6	8.27×10^6
Wave length	λ/L_{PP}	1.15	2.00	1.33
Wave height (m)	H_S	0.084	0.146	0.097
Encounter frequency (Hz)	fe	0.896	0.617	0.889

Fig. 2(a) and 2(b) show the grid generations around the KCS model. The ranges used for calculation were $-2.0 \le x/L_{PP} \le 2.0$, $0.0 \le y/L_{PP} \le 1.0$, and $-1.0 \le z/L_{PP} \le 0.5$. The position of forward perpendicular (F.P.) and after perpendicular (A.P.) of the hull were located at $x/L_{PP} = -1.0$ and $x/L_{PP} = 0.0$ at the still water free surface level ($z/L_{PP} = 0.046$) respectively. For the boundary conditions, the fluid velocity on the hull surface used the wall boundary condition, the entrance used the incident wave condition, the exit used the pressure boundary condition, and other boundary surfaces used the symmetric conditions of flow. The total number of grids was around 1.3 million. Although $y+ = 50$ was assumed to be the minimum interval of the grids vertical to the hull surface, the calculation indicated a distribution of $10 \le y+ \le 100$.

The number of grid points for wave length and wave height

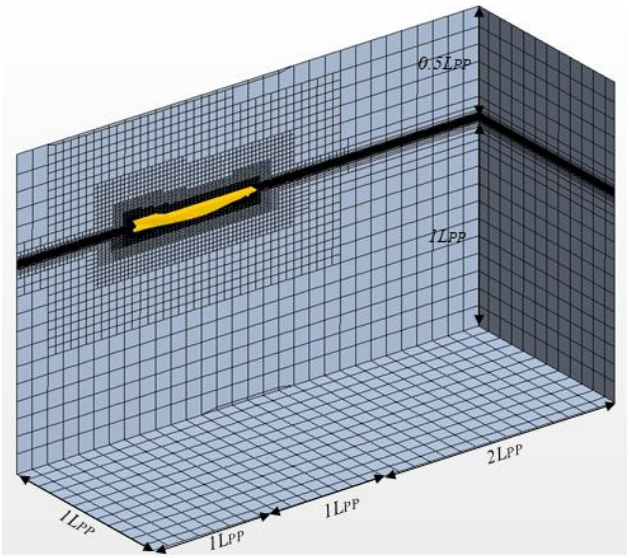

(a) Domain extensions for KCS

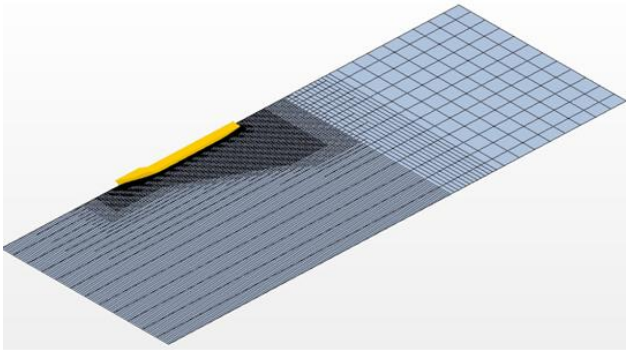

(b) Grid at the free surface for KCS

Fig. 2. Grid distribution around ship.

were distributed about the values of 67, 116 and 77 in x-direction per each wave length through C2, C3, and C4 incident wave conditions, respectively. Also in the z-direction, the grid points were spread about the values of 10, 16, and 10 per each amplitude respectively. The time interval was $\Delta t = 0.0025$. As the velocity field was developed around the hull, the heaving and pitching varied for 10 periods in a constant region. That corresponded to the time interval equivalent of 717, 945, and 771 times per period for each incident wave condition.

Fig. 3 shows the wave form condition at $t/T = 10$ under each incident wave condition. Numeric analysis indicated that the wave crest showed a wave amplitude difference of less than ±3 % as t/T changed while the wave trough showed a wave amplitude difference of around ±3 %. Moreover, the section from the exit to $L_{PP}/2$ was the wave damping section, meaning that the wave amplitude decreased.

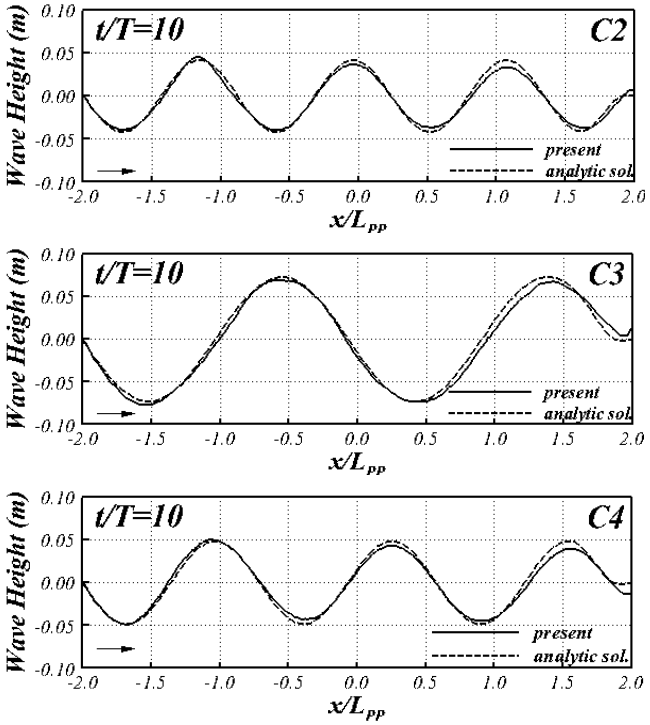

Fig. 3. Wave profile of C2, C3 and C4.

Table 3 shows the comparison of harmonic analysis of comparisons of the resistance coefficient, heave motion, and pitch angle per time change with the model test result. The resistance coefficients as well as the disposition of 0th amplitude and 1st amplitude show a big difference in terms of the model test in all incident wave conditions. Such a large gap in the resistance coefficient and disposition are consistent with the numeric analysis of other organizations that participated at the 2010 Gothenburg CFD Workshop.

The results of the first amplitude for the heave movement and pitch angle of harmonic analysis remained within ±20 % of the model test result. The difference from the model test result can be attributed to not only error in the numeric analysis, but also the different assumptions made, such as the center of gravity of the vessel, moment of inertia, and point of towing. Park et al. (2008) and Deng et al. (2010) also pointed out that the different initial conditions of the numeric analysis resulted in different vessel movements and dispositions.

3. Results

3.1 Motion Analysis

Fig. 4 and Table 4 show Motion analysis and the main specifications of the PSV observed in this study. Fig. 5(a) and 2(b) show the grid generations around the PSV model. The same calculation domain and boundary conditions as in the numeric analysis were used for verification. For the incident wave condition in Table 5, 156 grid points were distributed in the wave length x direction and 10 grid points were distributed in the wave amplitude z direction. The time interval of numeric analysis was $\Delta t = 0.001$. As the vortex field was developed around the hull, the heaving and pitching varied for 15 cycles in a specific section.

Table 3. Harmonic amplitudes and phase of the total resistance coefficient (C_T), heave motion, pitch angle for KCS

C_T		0th amplitude ($\times 10^3$)	1st amplitude ($\times 10^3$)	1st phase (°)
C2	EFD (S)	7.159	20.425	81.870
	CFD (D)	7.699	4.220	26.843
	E%D	-7.543	79.339	67.213
C3	EFD (S)	6.033	32.067	70.811
	CFD (D)	4.149	13.299	75.625
	E%D	31.228	58.527	-6.798
C4	EFD (S)	8.716	35.394	-260.205
	CFD (D)	8.709	4.339	-196.872
	E%D	0.080	87.741	24.340

Heave		0th amplitude (mm)	1st amplitude (mm)	1st phase (°)
C2	EFD (S)	-5.436	39.544	-20.566
	CFD (D)	-5.470	35.969	-14.347
	E%D	-0.625	9.041	30.239
C3	EFD (S)	-6.573	67.328	-3.095
	CFD (D)	-5.599	66.799	-34.896
	E%D	14.818	0.786	-1027.5
C4	EFD (S)	-12.274	61.811	-18.283
	CFD (D)	-11.920	51.280	-10.134
	E%D	2.884	17.037	44.571

Pitch		0th amplitude (°)	1st amplitude (°)	1st phase (°)
C2	EFD (S)	0.064	2.095	8.485
	CFD (D)	0.050	1.867	22.846
	E%D	21.875	10.883	-169.252
C3	EFD (S)	0.062	3.156	50.273
	CFD (D)	0.054	3.509	87.690
	E%D	12.903	-11.185	-74.428
C4	EFD (S)	-0.067	2.523	46.097
	CFD (D)	-0.082	2.019	43.736
	E%D	-22.388	19.976	5.122

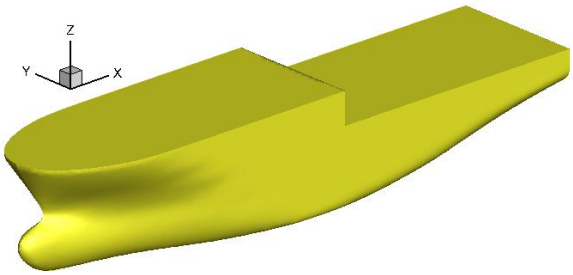

Fig. 4. PSV Model.

Table 4. Main particulars of the PSV

PSV (Scale ratio = 32.0)		
Length	L_{PP}	2.500 m
Draft	T	0.2031 m
Beam	B	0.6250 m
Wetted surface area	S_W	2.1575 m^2
Block coefficient	C_B	0.650
LCB (%L_{PP}), fwd+	-	-3.59
Moment of inertia	k_{XX}/L_{PP}	0.40
Moment of inertia	k_{YY}/L_{PP}, k_{ZZ}/L_{PP}	0.25

Table 5. Test case in regular waves for PSV

Condition		PSV
Speed (m/s)	V	1.455
Froude number	Fn	0.29
Reynolds number	Rn	3.62×10^6
Wave length	λ/L_{PP}	1.95
Wave height (m)	H_S	0.078
Encounter frequency (Hz)	fe	0.864

3.2 Motion Analysis result

Fig. 6 shows the resistance coefficient, heave motion, and pitch angle per time change. As the result of the heave motion and pitch angle shows, the time prior to the first encounter cycle was for fixing the full. In later cycles, the force and moment applied to the hull gradually increased and remained constant following the fifth encounter cycle. This phenomenon is attributed to the development of the vortex field around the hull to obtain calculation stability. The figure also shows a specific amount of settlement and trim by the bow with the center of gravity of the hull being the zero point. The settlement and trim by the bow at a constant forward moving speed in clear water was 0.015m and 0.894°, respectively. Similar settlement and trim by the bow were observed under the heave motion and pitch angle in regular waves by the forward moving

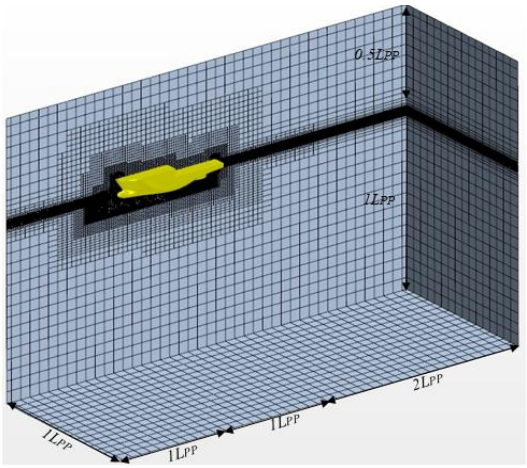

(a) Domain extensions for PSV

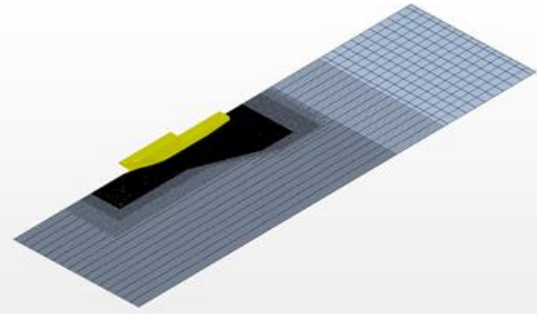

(b) Grid at the free surface for PSV

Fig. 5. Grid distribution around ship.

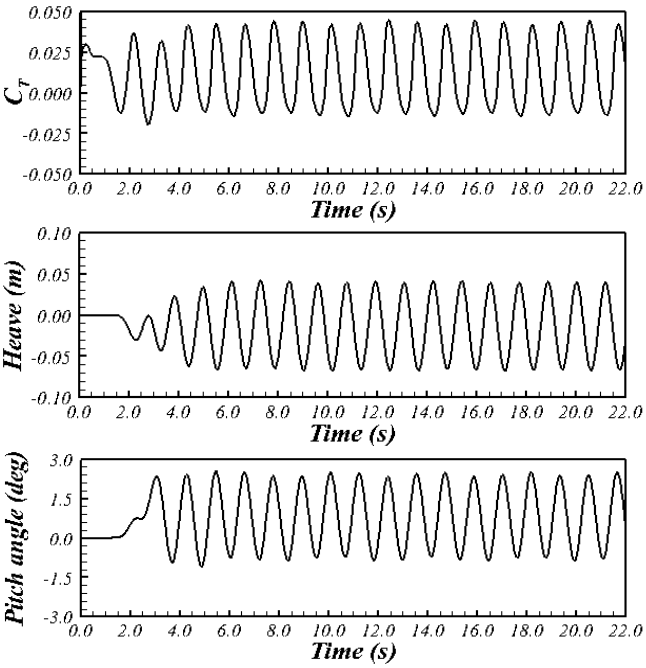

Fig. 6. Time histories of total resistance coefficient, heave motion, and pitch angle for PSV.

Table 6. Harmonic amplitudes and phase of the total resistance coefficient (C_T), heave motion, and pitch angle for PSV

C_T			
	0th amplitude ($\times 10^3$)	1st amplitude ($\times 10^3$)	1st phase (°)
CFD	11.636	28.207	72.783
Heave			
	0th amplitude (mm)	1st amplitude (mm)	1st phase (°)
CFD	12.054	44.042	109.929
Pitch			
	0th amplitude (°)	1st amplitude (°)	1st phase (°)
CFD	0.693	1.361	75.293

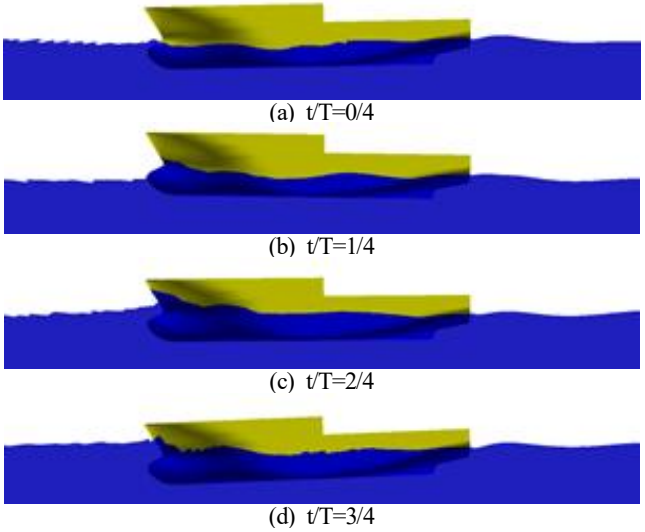

(a) t/T=0/4

(b) t/T=1/4

(c) t/T=2/4

(d) t/T=3/4

Fig. 7. Instantaneous free surface around ship at (a) t/T = 0/4, (b) t/T = 1/4, (c) t/T = 2/4, (d) t/T = 3/4.

vessel. Table 6 shows the harmonic amplitudes and phase of the resistance coefficient, while having motion and pitch angle per time change as a result of the numeric analysis.

Fig. 7 shows free surface wave patterns in period t/T = 0, 1/4 and 3/4. C_T and pitch values are largest at t/T = 0. Also, the maximum heave value was observed when the wave crest passed through around the mid-point of the ship. On the other hand, C_T and pitch are smallest at the A.P. position of the ship (t/T = 3/4).

4. Conclusion

This study analyzed the resistance and motion characteristic of a PSV in forward movement in regular waves. Verifying the numerical analysis technique used in this study, the results were compared with the model test result of KCS in the regular wave conditions and the analytic solution based on linear wave theory. In this study, each result indicated that the wave crest and wave trough showed a wave amplitude difference of less than ±3 % as t/T changed. The resistance coefficient and phase difference are consistent with those of previous studies published at the Gothenburg CFD Workshop (Larsson et al., 2010). For more accurate simulation, the initial conditions of the model test should be reflected in the numerical analysis (Carrica et al., 2006). Based on these CFD results, subsequent model EFD research including local flow investigation, is needed.

Acknowledgements

This work was supported by the Industrialization on the Ocean Convergence Materials Technology Development Program (No. 10053841, Green-Ship Superstructure Standard Unit Development with Fiber-based Composite Materials) funded by the Ministry of Trade, Industry and Energy (MOTIE) of Korea.

References

[1] Carrica, P. M., R. V. Wilson and F. Stern(2006), Unsteady RANS simulation of the Ship forward speed diffraction problem, Computers & Fluids, 35(6), pp. 545-570.

[2] Deng, G. B., A. Leroyer, E. Guilmineau, M. Queutey, M. Visonnau and J. Wackers(2010), Gothenburg 2010 A Workshop on Numerical Ship Hydrodynamics, Sweden, pp. 8-10.

[3] Korea Maritime Institute(2012), Measures to Encourage OSV (Offshore Support Vessel) Market Entrance for National Wealth Creation, Base Report No. 2012-04.

[4] Larsson, L., F. Stern and M. Visonneau(2010), Numerical Ship Hydrodynamics: An Assessment of the Gothenburg 2010 Workshop, Springer, 2013, in press.

[5] Otzen, J. F. and C. D. Simonsen(2008), Uncertainty assessment for KCS resistance and propulsion tests in waves, FORCE Technology Report No ONRⅢ187-01.

[6] Park, K. S.(2015), Forecast of Offshore Support Vessel (OSV) and our strategies, The Korean Society for Marine Environment & Energy, Proceedings of KAOSTS 2015, p. 135.

[7] Park, I. R., K. S. Kim, J. Kim and S. H. Van(2008), Unsteady RANS Analysis of the Hydrodynamic Response for

a Ship with Forward Speed in Regular Wave, Journal of the Society of Naval Architects of Korea, 45(1), pp. 29-41.

[8] Tahara, Y. and J. Ando(2000), Comparison of CFD and EFD for KCS container ship in without/with propeller conditions, In: Gothenburg: A Workshop on Numerical Ship Hydrodynamics, Chalmers University of Technology, Gothenburg, Sweden.

[9] Yum, J. G., K. J. Kang, Y. Y. Lee, C. J. Lee and K. D. Ok(2018), A Study on the Basic Design for Platform Support Vessel (PSV) and Hull Form Development for Enhancement of Resistance & Propulsion Performance, Journal of the Society of Naval Architects of Korea, Vol. 55, No. 3, pp. 196-204.

Received : 2019. 04. 23.
Revised : 2019. 05. 23.
Accepted : 2019. 05. 28.